Journal of Catalysis **185,** 91–105 (1999)
Article ID jcat.1999.2484, available online at http://www.idealibrary.com on IDEAL®

Efficient Stable Catalysts for Low Temperature Carbon Monoxide Oxidation

G. G. Xia,*,‡ Y. G. Yin,*,[2] W. S. Willis,*,‡ J. Y. Wang,* and S. L. Suib*,†,‡,[1]

*Department of Chemistry, U-60, †Department of Chemical Engineering, and ‡Institute of Materials Science, University of Connecticut, Storrs, Connecticut 06269-4060

Received October 1, 1998; revised March 15, 1999; accepted March 16, 1999

Octahedral molecular sieves (OMS), doped with Ag^{+}, Co^{2+}, and Cu^{2+}, have been tested for their catalytic activity for carbon monoxide oxidation at low temperatures for long times on stream. Metal loaded OMS materials are highly active for this catalytic reaction and compare favorably with other catalysts such as Hopcalite-like $CuMn_2O_4$ catalysts, supported Ag catalysts, and supported noble-metal catalysts, especially with respect to resistance to deactivation in a long run. Co-doped OMS-2 has been tested for selective oxidation in the presence of a large surplus of hydrogen in the feed gas. This catalyst shows nearly exclusive oxidation of CO versus hydrogen with oxygen present in stoichiometric amounts with carbon monoxide. Its stability against reduction in CO or H_2 containing gas is demonstrated from comparisons of X-ray diffraction patterns and X-ray photoelectron spectra before and after exposure to these gases. Average oxidation numbers and populations of Mn valence states were determined for these catalysts. Catalytic activity of doped OMS catalysts toward CO oxidation shows a correlation among average oxidation number of Mn and the position and nature of the doped cation. The structure of the active sites and the mechanism of the reaction are proposed.

Key Words: **CO oxidation; low temperature; octahedral molecular sieve (OMS); manganese oxide catalyst; average oxidation number; electron charge transfer.**

I. INTRODUCTION

Carbon monoxide as a toxic component of air has long been targeted for removal from air. Catalytic oxidation is the most effective means for its removal. Hopcalite (a Cu–Mn mixed oxide) has been the oldest catalyst widely used for respiratory protection systems in many types of applications (1–3). Applications in military, mining, and space devices have led to studies of the preparation and characterization of Cu–Mn oxide systems (4–8). Improvement in activity of metal catalysts for CO oxidation has been attempted by combining manganese with other elements. Such examples are Ag/Mn catalysts (9–11), and perovskite-type manganite catalysts (12, 13).

Interest in the catalytic oxidation of carbon monoxide has surged due to possible applications in orbiting, closed-cycle CO_2 lasers used for weather monitoring and other remote sensing applications (14, 15). Closed-cycle CO_2 lasers produce CO and O_2 in the laser discharge resulting in a rapid loss of output power. Catalysts are needed to convert CO and O_2 back to CO_2. Such catalysts also find applications in CO detecting sensor devices. Instead of mixed oxide catalysts, recent studies have focused on supported noble metals. For example, Haruta *et al.* (16–19) were the first to report on supported gold catalysts, followed by Knell *et al.* (20), Hoflund (14, 15, 22, 23), Upchurch (21) and co-workers (14, 15, 21–23), and Vannice and co-workers (24–30) studied a series of supported Pd, Cu, and Pd–Cu catalysts, as well as TiO_2 supported Au catalysts for low-temperature oxidation of carbon monoxide. A majority of these catalysts (mixed oxides and supported noble metal catalysts) deactivate over a few hours. Grunwaldt and co-workers (31, 32) have systematically studied ZrO_2 and TiO_2 supported gold catalysts for low temperature CO oxidation. They found that the particle size of gold colloids and supports are very important parameters for CO oxidation.

Both Mn complex oxides and supported noble metal catalysts have been characterized by several physico-chemical methods. However, the most notable method for correlation of structure and activity seems to be correlation of catalytic activity for CO oxidation and active oxygen content of Mn in oxide catalysts (5).

Recent interest has focused on preparation of CO oxidation catalysts that are active in the presence of large amounts of H_2 in the feed gas. This is related to the use of hydrogen for energy sources in fuel cells, due to the presence of very small amounts of CO in the hydrogen from the water–gas–shift reaction which causes poisoning of the fuel cell electrodes. This imposes a tough challenge for oxidation catalysts (33). This problem is even more challenging if oxygen is added in stoichiometric amounts to CO and when significant amounts of water vapor are present.

Manganese has been a component of many oxidation catalysts, especially in Hopcalite-like compounds. Many studies have been devoted to studying catalytic effects in oxidation (especially for CO) of Mn in various

[1] To whom correspondence should be addressed.
[2] Current address: Sabic Technology Center, 16200A Park Row, Houston, TX 77804.

0021-9517/99 $30.00

crystallographic sites. Manganite perovskites have been extensively studied in this aspect. Very recently, catalytic activity of murdochites (M_6MnO_6) toward CO oxidation was reported (34). However, there are no reports of the activity of these Mn complex oxides with respect to CO oxidation.

Octahedral molecular sieves (OMS) have been found to exhibit high activity for oxidation reactions, including carbon monoxide oxidation (35). The major goal of this study was to find the best performance of doped OMS catalysts at as low a temperature and as high a space velocity as possible. X-ray diffraction (XRD) and X-ray photoelectron spectroscopic (XPS) studies have been pursued to further understand the stability of such catalysts after reaction in $CO + O_2$ mixtures and/or after exposure to H_2 containing gases. The behavior toward competition of CO oxidation versus hydrogen oxidation has also been explored. Activation energies of CO oxidation over several transition metal loaded OMS catalysts were derived from Arrhenius plots. The population of Mn in different valence states was determined and such electronic effects on catalytic activity in CO oxidation were studied.

II. EXPERIMENTAL

(1) Reactor System

A mixed gas tank of 2% $CO + 1\%$ O_2 in He was purchased as moisture-free from Connecticut Air-Gas Company. In most of the experiments the feed gas was further dried by passing through a 10-cm length bed of drierite and a 10-cm length bed of 4A molecular sieve. A separate gas tank of 30% H_2 in He was purchased and used to evaluate the competitive oxidation of CO and H_2.

A few experiments at initial stages used a U-tube of internal diameter 4 mm as a reactor. In most of the experiments, a two-piece U-tube reactor was used. Catalyst samples were packed in one end of a 1/4″ Pyrex tube with a side arm for exit of gas, which was inserted into and sealed to a 1/2″ U-tube with a Swagelok reducing union. Such a two-piece U-tube reactor facilitates loading and unloading of catalyst samples in a narrow glass tube. Weights of catalyst samples for 0°C run were 119.7–120.8 mg; those for 35°C were 57.1–60.5 mg (except that of catalyst Cu–C which was 80.1 mg); those for 60°C run were 79.6–80.4 mg (except those of catalysts Ag–B and Co–A which were both 40.1 mg); and those for 100°C run were 39.8–40.6 mg (except those of catalysts Ag–C and Co–E which were 59.9 and 80.7 mg, respectively). The reactor was either placed in a fluidized bed heater or ice-water bath to ensure uniform temperature distribution and rapid dissipation of the heat of reaction. Change in catalyst activity was studied at times on stream between 10 and 50 h. Each experiment involved fresh catalyst for different test conditions. The sample was treated in flowing air (20 ccm) at 180°C for 2 h and then purged with He stream (20 ccm) before activity tests. When the reactor temperature was cooled to a designated reaction temperature, He purging was further conducted for 15 min at this temperature. After that, a mixture of 2% $CO + 1\%$ O_2 in He was introduced to the reactor at a given space velocity. The gas stream was controlled with a mass-flow controller. With competitive oxidation experiments, the above gas mixture and 30% H_2/He were introduced into the reactor at a specific ratio, also controlled with a mass-flow controller. The space velocity of the feed gas was expressed as volume of total feed gas passed per hour per unit weight of catalyst, vwh. The space velocity for runs at 60 and 100°C was not fixed in order to optimize catalyst performance. Repeatability was generally satisfactory. For example, over a Cu–C catalyst at 60°C and around 2000 vwh, one run from 15–27 h time on stream gave an average CO conversion of $36.4 \pm 2.2\%$; while another similar run in the same period of time on stream gave an average CO conversion of $38.0 \pm 2.5\%$. Over a Co–A catalyst, at 100°C and 9500 vwh, one run gave an average CO conversion of $60.8\% \pm 2.0\%$ over 2–25 h time on stream. Another run gave $59.4 \pm 0.7\%$.

(2) Analysis of Reaction Products

Reactor effluents were analyzed with a Hewlett-Packard 5890 II gas chromatograph, using a Carboxen 1000 (Supelco product) packed column at 100°C with a thermal conductivity detector (TCD). Peaks for H_2, O_2, N_2, CO, CH_4, and CO_2 were well separated and their peak areas were quantified with a Hewlett-Packard 3396 II integrator. Response factors for all the gases, except H_2, were applied (36). For H_2, no accurate response factor has been reported, and a calibration value for H_2 was obtained by standardization with pure H_2 and certified 5% H_2/Ar.

(3) Catalyst Preparation

From preliminary experiments, it was observed that OMS catalysts are active for CO oxidation when Co^{2+}, Ag^{+}, or Cu^{2+} were incorporated into OMS with the cryptomelane-structure (OMS-2). Emphasis was focused on these doped OMS-2 materials, prepared with a variety of methods. Catalysts made by incorporating cations into OMS with the todorokite-structure (OMS-1) or other OMS-2 are also presented for comparison.

The doped OMS-1 catalysts were prepared by autoclaving a reaction mixture of $KMnO_4$ and $MnSO_4$, with addition of appropriate metal salts (37). The doped OMS-2 catalysts were prepared by redox reactions of solutions of $KMnO_4$ and $MnSO_4$ with a priori (before refluxing or calcination to OMS-2 structure) (38) or a posteriori (ion-exchanging or homogeneous precipitation with urea after formation of the OMS-2 structure) incorporation of Ag^{+}, Co^{2+}, Cu^{2+}, or other cations. The mono/divalent transition metal cations mostly situate in framework positions of the OMS-2

TABLE 1

Designation of Catalysts Used

Catalyst	Cations incorporated	Mode of preparation	Surface area, m^2/g
Cu–A	Cu^{2+} in OMS-2	A priori, add higher concentration of $Cu(NO_3)_2$ before refluxing.	73
Cu–C	Cu^{2+} in OMS-2	A priori, add low concentration of $Cu(NO_3)_2$ before refluxing.	60
Co–A	Co^{2+} in OMS-2	A priori, add high concentration of $Cu(NO_3)_2$ before refluxing.	66
Co–B	Co^{2+} in OMS-2	Homogeneous precipitation of $Co(NO_3)_2$ in presence of K–OMS-2.	39
Co–C	Co^{2+} in OMS-2	A posteriori, ion-exchanging with $Co(NO_3)_2$.	51
Co–E	Co^{2+} in OMS-1	A priori, add $Co(NO_3)_2$ before autoclaving.	16
Ag–A	Ag^{+} in OMS-2	A posteriori, high-temperature ion exchanging vs $AgNO_3$.	52
Ag–B	Ag^{+} in OMS-2	A posteriori, low-temperature ion exchanging vs $AgNO_3$.	54
Ag–C	Ag^{+} on OMS-1	A priori, add $AgNO_3$ before autoclaving.	22
K–OMS	K^{+} on OMS-2	As prepared.	69
Fe–OMS	Fe^{2+} in OMS-2	A priori, add $Fe(NO_3)_3$ before refluxing.	67

structure for the catalysts with a priori incorporation. In a posteriori incorporation, the cations situate in either tunnel positions (if prepared by ion-exchange) or in extra-framework positions (if prepared by homogeneous precipitation) (37, 39). Catalysts used in this paper are described in Table 1, where the type of OMS structure, the cations incorporated, mode of incorporation of cations, and other parameters are described.

(4) Analysis of Catalysts

Total manganese was analyzed after dissolution of all of the Mn in the sample with concentrated HCl as Mn^{2+}. The Lingane–Karplus method, i.e., potentiometric titration with standard $KMnO_4$ to Mn^{3+}, stabilized by the presence of a large excess of pyrophosphate ion, was used for these studies. The determination of Mn^{2+} in samples was done by extracting Mn^{2+} with 3 M ammonium sulfate solution from the solid sample, according to a study by Parida (40), and then potentiometrically titrating the extracted Mn^{2+} with $KMnO_4$. The determination of Mn^{3+} was done similarly, except a 6 M HNO_3 solution was used to extract Mn^{3+} from the sample. In this case, there is an immediate disproportionation of Mn^{3+} to Mn^{2+} and Mn^{4+} after dissolution, and the Mn^{2+} was determined as mentioned above. The Mn^{4+} content was determined from the difference between total Mn and $(Mn^{2+} + Mn^{3+})$ content. The average oxidation number of manganese was determined by titrating an excess of Fe^{2+} with $KMnO_4$, after reacting the solid samples with a known amount of $Fe(NH_4)_2(SO_4)_2$ solution until the appearance of a pink coloration of $KMnO_4$ (41).

(5) Surface Area Measurements

Surface areas of the tested catalyst samples were measured in a NOVA-1000 Gas Sorption BET unit, using a 5-point BET method for nitrogen adsorption; see Table 1. Samples were heated to 120°C prior to analysis.

(6) X-ray Powder Diffraction Patterns

XRD patterns of some Co–, Ag–, and Cu–OMS-2 catalysts, before and after long times on stream, were collected by using a Scintag 2000 XDS diffractometer with Cu $K\alpha$ X-ray radiation. A 0.02 step in 2θ/count and beam voltage of 45 kV and beam current of 40 mA were used. JCPDS powder diffraction data files were used as references for phase identification of hollandite/cryptomelane. The X-ray diffraction patterns of fresh and treated OMS-2 were displayed and stacked via IGOR software.

(7) XPS Studies

XPS of a Co–OMS-2 catalyst was studied in a Leybold instrument equipped with a SPECS EA10MCD electron energy analyzer. Data for all detailed spectra were acquired using a Mg X-ray anode (1253.6 eV) and a constant energy analyzer pass energy of 59.21 eV. The pressure was kept below 1×10^{-8} mbar during data acquisition. Co–OMS-2 was pressed into In foil for XPS analysis. After analyzing the untreated sample, the sample was moved to a side chamber where the CO gas mixture ($CO : O_2 : He = 2 : 1 : 97\%$) or 5% H_2/Ar gas, at 10 ccm, was passed over the sample for 1 h at 35°C. The sample was then returned to the main chamber for a post-treatment analysis. XPS data of fresh and treated OMS-2 were displayed and overlaid via IGOR software.

(8) Determination of Activation Energies for CO Oxidation

Differential reaction rates of CO oxidation over Co–A, Co–E, Cu–A, Cu–C, Ag–A, and Ag–C catalysts were run at several different temperatures from 35 to 100°C. The feed gas and reactor used are the same as mentioned above. CO conversion was limited to below 10% by the varying flow rate of the feed gas and the weight of catalysts. Activation energies can be determined from Arrhenius plots.

III. RESULTS

The reactor containing an appropriate weight of catalyst was placed in a constant temperature bath of ice-water. Results of the catalytic oxidation of CO at 0°C for Ag–A, Co–A, and Cu–C (each with space velocity around 1000 vwh

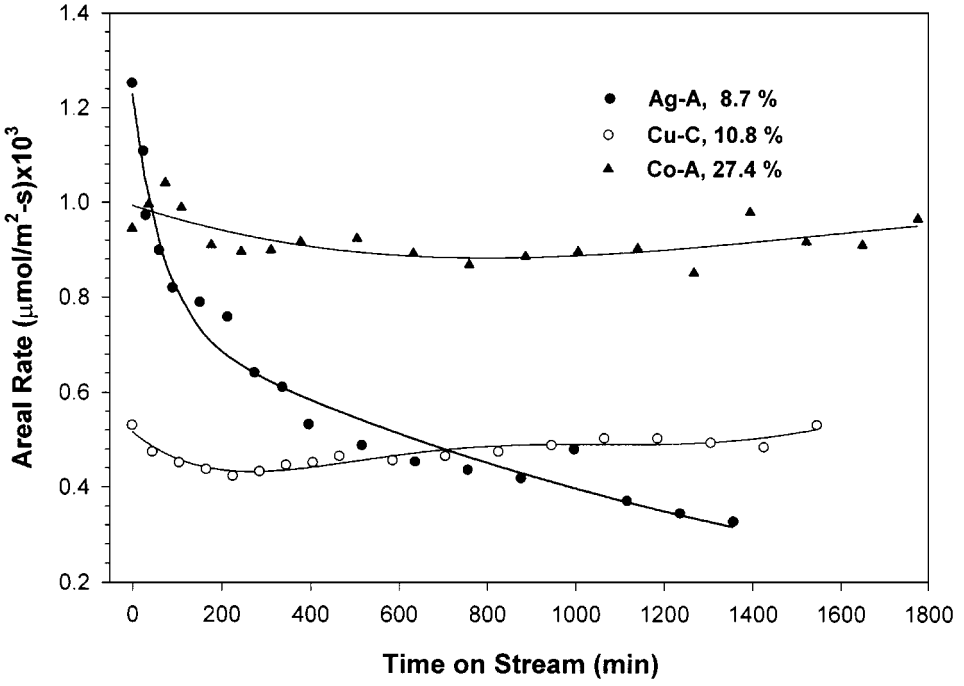

FIG. 1. Plots of areal rates of CO oxidation over doped OMS catalysts vs time on stream at 0°C and 1000 vwh; the percentages are average conversions at steady state.

and extended over 25 to 30 h) are shown in Fig. 1. The areal rate of a given catalyst for CO oxidation is defined as the moles of CO oxidized per unit surface area of catalysts per unit time.

CO oxidation over Ag–B, Co–A, Co–B, Co–C, Cu–C, and Co–E catalysts at 35°C were conducted in a fluidized bed reactor at a space velocity around 3000 vwh over a 25–50 h period. These catalytic results are presented in Fig. 2. The

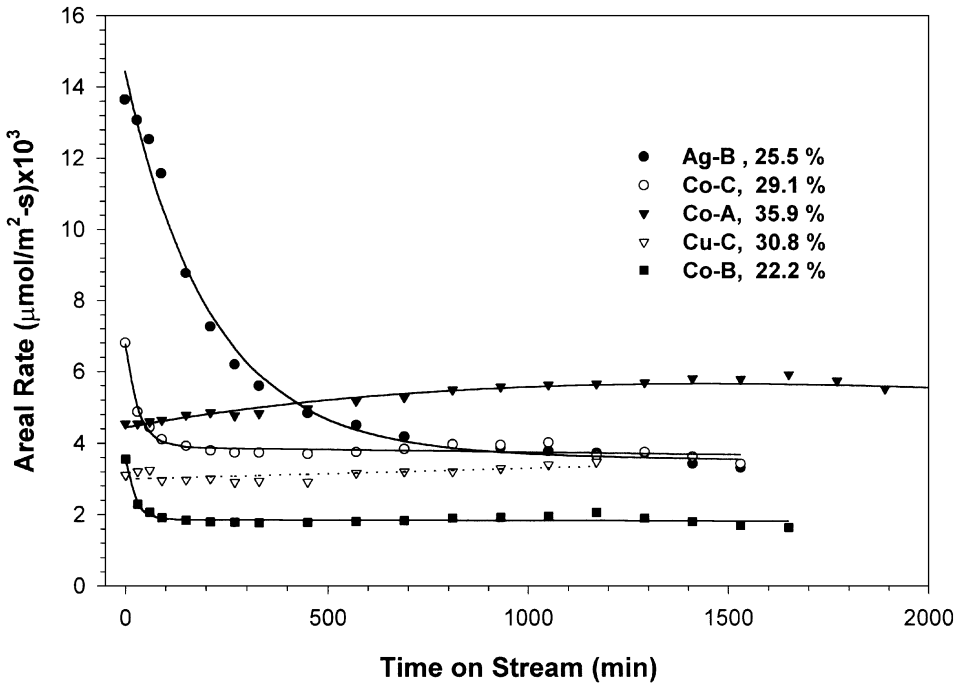

FIG. 2. Plots of areal rates of CO oxidation over doped OMS catalysts vs time on stream at 35°C; the percentages are average conversions at steady state.

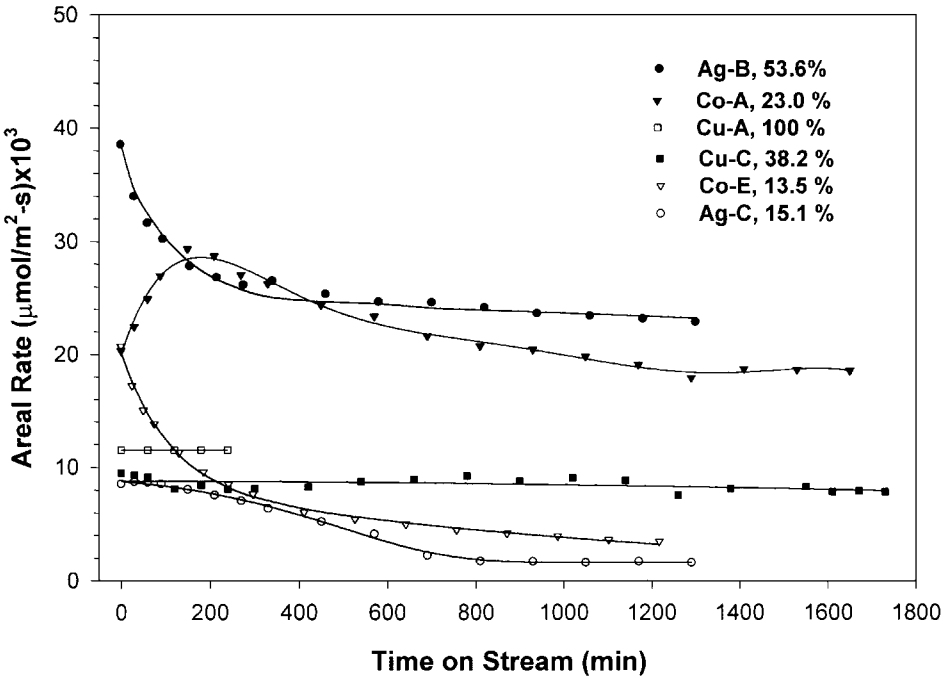

FIG. 3. Plots of areal rates of CO oxidation over doped OMS catalysts vs time on stream at 60°C and 1000 vwh; the percentages are average conversions at steady state. Ag–B, 11,500 vwh; Ag–C, 1240 vwh; Co–A, 25,700 vwh; Co–E, 2140 vwh; Cu–A, 2250 vwh; Cu–C, 2540 vwh.

conversion level for catalyst Co–E was only 3% and is not presented in this figure.

Activity tests at 60°C for doped OMS-1 and OMS-2 catalysts were also conducted in a fluidized bed reactor. Results for Ag–B, Ag–C, Co–A, Co–E, Cu–A, and Cu–C catalysts are shown in Fig. 3. The catalysts were tested at different space velocities (1240–26,500 vwh) in order to obtain comparable conversions for CO oxidation over different catalysts. Due to the rather low activity of doped OMS-1 materials (Ag–C and Co–E), experiments for these catalysts

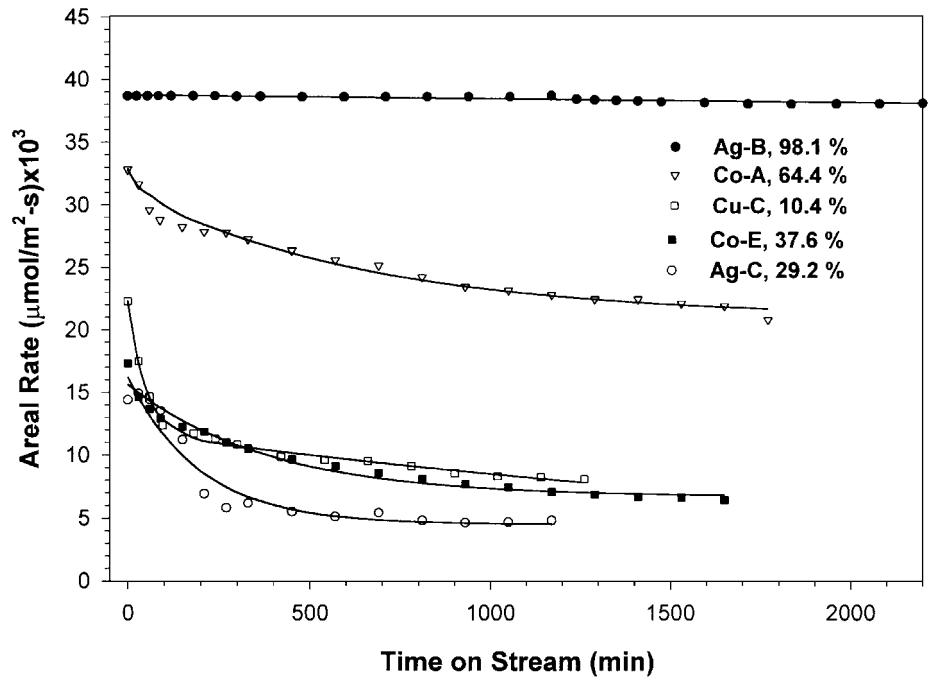

FIG. 4. Plots of areal rates of CO oxidation over doped OMS catalysts vs time on stream at 100°C; the percentages are average conversions at steady state. Ag–B, 11,510 vwh; Ag–C, 2000 vwh; Co–E, 1580 vwh; Cu–C, 26,500 vwh; Co–A, 9000 vwh.

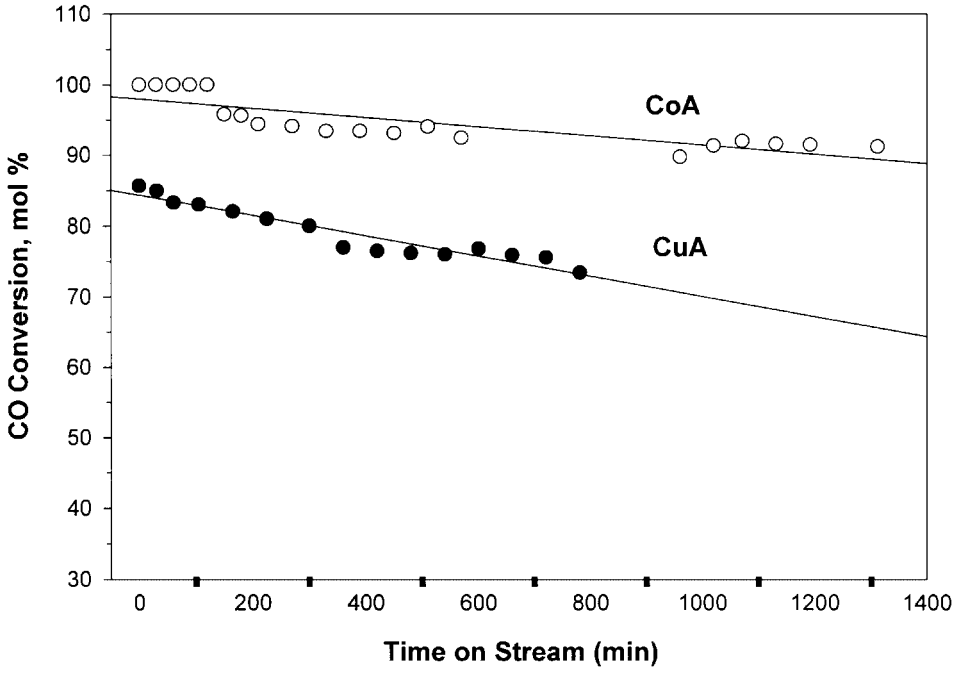

FIG. 5. CO conversion over Co–A and Cu–A catalysts in presence of H_2: Feed gas, 1% CO, 0.5% O_2, 30% H_2 in He; Temperature, 100°C; Space velocity, 6400 vwh for Co–A and 3600 vwh for Cu–A.

had to be run at reduced space velocity. These two doped OMS-1 catalysts are a good contrast to doped OMS-2 materials. The undoped OMS-2 (K–OMS-2) materials show no activity for CO oxidation at 60°C even at 7800 vwh.

CO oxidation at 100°C for doped OMS-1 and OMS-2 catalysts were conducted in a fluidized bed reactor. Results for Ag–B, Ag–C, Co–A, Co–E, and Cu–C at 100°C are shown in Fig. 4. The activity of Fe–OMS-2 at 100°C and at a space velocity of 5400 vwh is too low to be shown in this figure. The areal rate of CO oxidation over Ag–B at 100°C and 11,500 vwh changes slowly. The areal rate of CO oxidation over Co–A at 100°C and 9000 vwh drops about 30% within 30 h. The two transition metal loaded OMS-1 materials show very low areal rates for CO oxidation. Cu–C exhibits a relatively higher initial areal rate as compared to the two M–OMS-1 catalysts, but decreases sharply within 3 h.

Co–A and Cu–A were tested for competitive oxidation of CO against H_2 at 100°C with a feed gas containing 1% CO, 0.5% O_2, and 30% H_2 in He. The results are shown in Fig. 5. The selective conversion of CO over Co–A, at a space velocity of 6400 vwh changes from 100 to 91.1% within 25 h. At a space velocity of 3500 vwh the conversion of CO is steady at 94–98% over 4 h. Over Cu–A catalysts at 100°C, the CO conversion is initially 85.7% and becomes steady at 76.4% after 10 h. Methane and water were not detected in the product stream. Arrhenius plots for CO oxidation over Co–A, Co–E, Cu–A, Cu–C, Ag–A, and Ag–C catalysts are shown in Fig. 6.

XRD patterns of Co–A, Ag–B, and Cu–A catalysts, before and after long times on stream for oxidation of CO, are shown in Fig. 7. Figure 8 compares X-ray photoelectron Mn 2*p* spectra of the Co–A catalyst before and after exposure to $CO + O_2$ gas mixture for 1 h in a side chamber of the XPS instrument. Figures 9 and 10 show the Co 2*p* and O 1*s* spectra, respectively, of Co–A before and after exposure to $CO + O_2$. As the Mn 2*p*, Co 2*p*, and O 1*s* spectra of Co–A before and after exposure to H_2/Ar are exactly the same as those corresponding spectra for samples exposed to $CO + O_2$, they are not displayed in this paper. Figure 11 shows the Mn 3*s* spectra of Co–A before and after exposure to H_2/Ar.

The analytical results for manganese valence state populations and average oxidation numbers of most of the doped OMS catalysts are shown in Table 2. The activation energies

TABLE 2

Mn Valence Distribution of Doped OMS (in mmol/g)

Sample	Mn^{+2}	Mn^{+3}	Mn^{+4}	Average oxidation number	
				Calcd.	Anal.
Ag–C	0.075	3.37	5.96	3.626	3.262
Co–E	0.010	3.96	4.56	3.532	3.574
Co–A	0.012	0.30	8.46	3.962	N/A[a]
Cu–C	0.005	0.49	8.76	3.946	3.908
Cu–A	0.005	0.26	9.97	3.974	3.912

[a] Not analyzed.

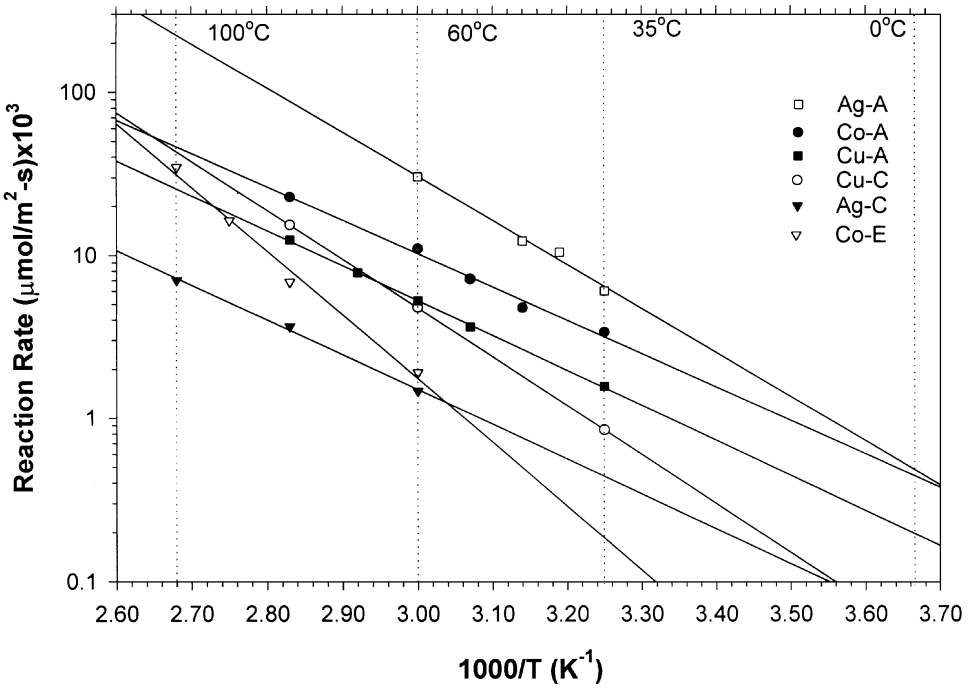

FIG. 6. Arrhenius plots for M–OMS catalysts. CO conversions were limited to under 10% by varying the flow rate of the feed gas (2% CO + 1% O_2 in He) and/or the weight of catalysts.

over these catalysts and reaction rates under various temperatures which can be derived from these plots are shown in Table 3. The correlation between reaction rates of CO oxidation over different OMS catalysts and the average oxidation number of manganese is plotted as Fig. 12.

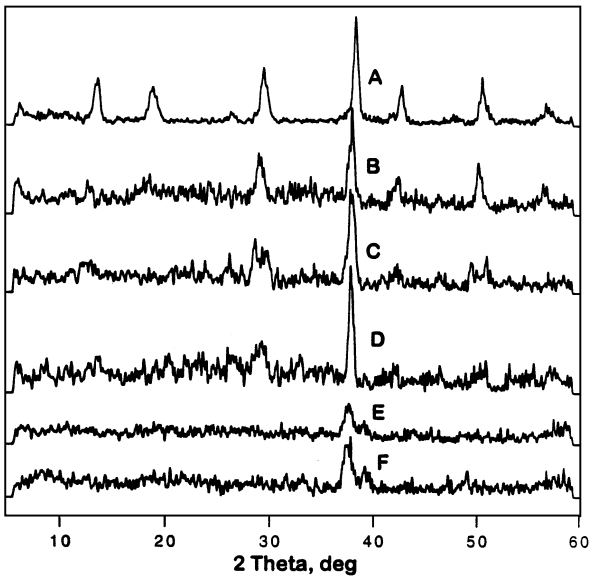

FIG. 7. Comparisons of XRD patterns of doped OMS-2 catalysts before and after catalytic reaction: A, Co–A before reaction; B, Co–A after reaction; C, Ag–B before reaction; D, Ag–B after reaction; E, Cu–A before reaction; F, Cu–A after reaction.

IV. DISCUSSION

A. *Low-Temperature Performance*

It is clear from the data of Figs. 1 and 2 that transition metal loaded OMS-2 (Co–A, Co–B, Co–C, Ag–A, Ag–B, and Cu–C) catalysts show noticeable areal rates toward CO oxidation at ambient or lower temperatures. Even at

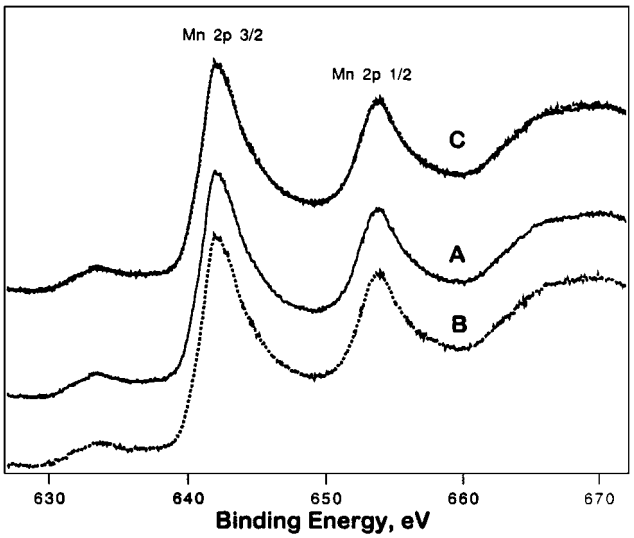

FIG. 8. Comparisons of XPS of Co–A Mn 2*p* before and after exposure to CO + O_2: A, Mn 2*p* spectra before exposure; B, Mn 2*p* spectra after exposure; C, overlay of A and B.

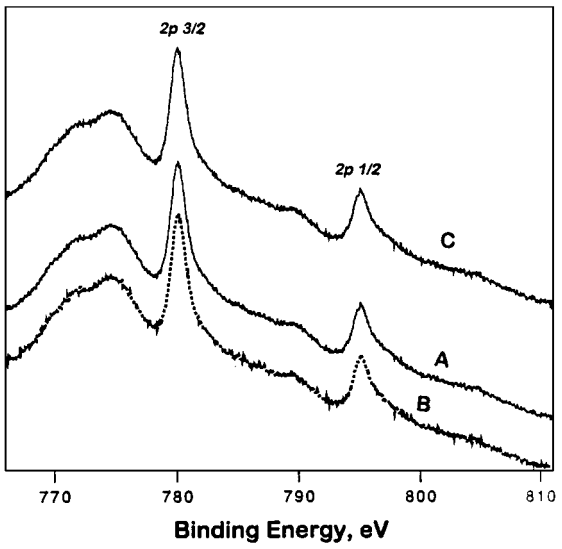

FIG. 9. Comparisons of XPS of Co–A CO 2*p* before and after exposure to $CO + O_2$: A, Co 2*p* spectra before exposure; B, Co 2*p* spectra after exposure; C, overlay of A and B.

0°C, the high concentration of cobalt loaded OMS-2, Co–A, shows a higher average areal rate for CO oxidation and a higher conversion than the other two catalysts under similar experimental conditions. The conversion of CO over Co–A is about 27%, which is stable for about 30 h at a space velocity near 1000 vwh. In contrast, Ag–A (Ag^+ exchanged OMS-2 at high temperature) under similar conditions shows similar initial areal rates, but it decays considerably over 25 h time on stream. The low concentration of Cu-doped OMS-2 (Cu–C) shows much lower activity at 0°C, although its activity remains stable after 27 h time on stream. At 35°C, both Co–A and Cu–C show slow changes in areal rates for CO oxidation during the tests. Ag–B (Ag^+ exchanged OMS-2 at low temperature) exhibits the highest initial areal rate for CO oxidation among the tested catalysts, but the areal rates decay quickly as reaction time increases. Among the three Co-doped OMS-2 systems, Co–B, where Co^{2+} was deposited in extra-framework sites of OMS-2 by homogeneous precipitation, shows the lowest catalytic activity at 35°C. This suggests that the concentration of loaded transition metal cations and the mode of doping the OMS framework play a significant role in these CO oxidation catalysts. Differences in activity of Co–A and Co–C are related to effects of the mode of incorporation of Co^{2+}.

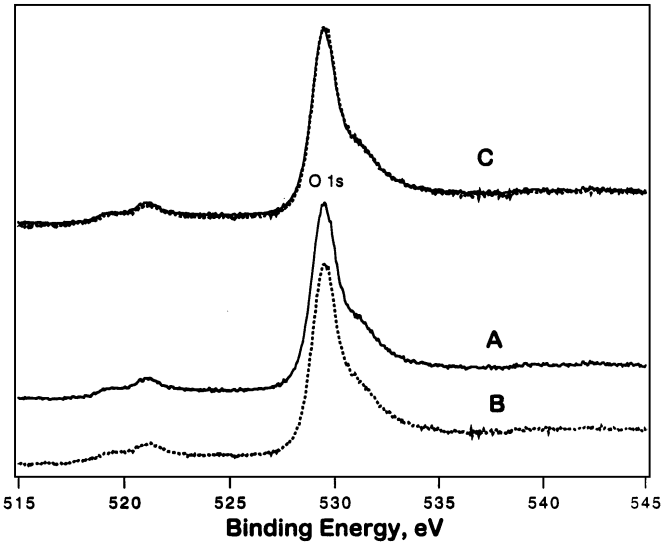

FIG. 10. Comparisons of XPS of Co–A O*s* before and after exposure to $CO + O_2$: A, O 1*s* spectra before exposure; B, O 1*s* spectra after exposure; C, overlay of A and B.

In a study reported by Puckhaber (7), Cu–Mn mixed oxide catalysts were compared with a commercial Hopcalite catalyst at 25°C. Although 100% conversion of CO was achieved initially, the conversion dropped sharply after 30–60 min time on stream and finally decreased to 0%. Kanungo (5) reported studies of catalytic activity of a variety of $CuO–MnO_2$ mixed oxides. The CO conversion was highest at 17.1% for a MnO_2 system onto which $Cu(OH)_2$ was precipitated at 40°C.

Supported noble metal catalysts seem to be quite active for CO oxidation at low temperatures. Haruta *et al.* (17) reported that a 12% Au/α-Fe_2O_3 catalyst gave 100% conversion of CO at 0°C. Knell *et al.* (20) reported that a 10 mol% Au/ZrO_2 catalyst gave complete conversion of CO at room temperature.

Doped OMS-2 catalysts show much higher activity for CO oxidation than traditional Cu–Mn mixed oxide catalysts and result in satisfactory activity toward CO oxidation even at low temperatures. However, they are not as active as Au/MnO_x catalysts (17).

B. High-Temperature Performance

Some of the doped and ion-exchanged OMS-2 catalysts show very high catalytic activity for CO oxidation at temperatures slightly above ambient temperature. At 60°C, as shown in Fig. 3, Ag-, Co-, and Cu-loaded OMS-2 are good catalysts for this reaction, even at rather high space velocities. Cu-doped OMS-2 (Cu–A) shows sustained areal rates at 60°C for complete oxidation of CO over a 4 h time on stream at a space velocity of 2250 vwh. At higher space velocities, all other Ag-, Co-, and Cu-doped OMS-2 catalysts show decreasing catalytic activity. Note that the areal rate of CO oxidation over Ag–B is higher than the other materials. On the other hand, high concentrations of cations in doped OMS-2 (Co–A and Cu–A) catalysts have a higher catalytic activity in comparison to their low concentration cation doped analogs (Cu–C). Ag- and Co-doped OMS-1 (Ag–C and Co–E, respectively) are of lowest average areal rates among the catalysts tested although Co–E shows a

TABLE 3

CO Oxidation Rate under Various Reaction Temperatures

Catalyst	Description[a]	Average oxidation number	E_a (kJ/mol)	$r \times 10^9$ (mol · m^{-2} · s^{-1})			
				273 K	308 K	333 K	373 K
Co–A	Co–OMS-2 (H)	3.962	39	0.45	3.18	10.1	46.1
Cu–C	Cu-OMS-2 (L)	3.946	57	0.05	0.79	4.64	42.8
Cu–A	Cu-OMS-2 (H)	3.974	41	0.19	1.55	5.17	25.4
Ag–A	Ag-OMS-2 (Ex)	—	52	0.49	6.52	29.7	221
Ag–C	Ag-OMS-1	3.626	41	0.06	0.45	1.47	7.18
Co–E	Co-OMS-1	3.532	75	0	0.19	1.70	30.9

[a] H, high concentration of transition metal dopant; L, low concentration of transition metal dopant; Ex, cation-exchanged transition metal.

high initial areal rate for CO oxidation, as shown in Fig. 3. K–OMS-2 shows negligible activity at 60°C. These data again show the effects of concentration of doped transition metal cations. These results show that a cryptomelane 2×2 tunnel structure is necessary for high CO oxidation activity. This may be due to shape selective effects of the smaller tunnel 2×2 structure in comparison to the larger tunnel 3×3 structure. Furthermore, the concentrations of loaded cations and their mobility (ion-exchanged compared with doped OMS-2) may also play important roles in CO oxidation.

At 100°C, Ag–B shows excellent catalytic ability toward CO oxidation. Nearly complete conversion of CO over the Ag–B catalyst at 11,500 vwh for 20 h was obtained. Co–A also shows a rather high areal rate and conversion at 9000 vwh. At 35 and 60°C, Cu–C shows quite steady activity, as mentioned above. However, Cu–C suffers noticeable deactivation at a higher space velocity (26,500 vwh) at 100°C within a 3 h period (see Fig. 4). These transition metal loaded OMS-1 materials (Co–E and Ag–C) still have lower areal rates for CO oxidation than M–OMS-2 catalysts.

Kanungo has reported that a mixed $CuO–MnO_2$ catalyst mentioned in the last section (IVA) gave a conversion of CO of 45.5% at 80°C (5). Taguchi *et al.* (34) recently reported the oxidation of CO on murdochite-type $(Mg_{6-x}Al_x)MnO_8$ catalysts. Both Mg^{2+} and Mn^{4+} ions are octahedrally

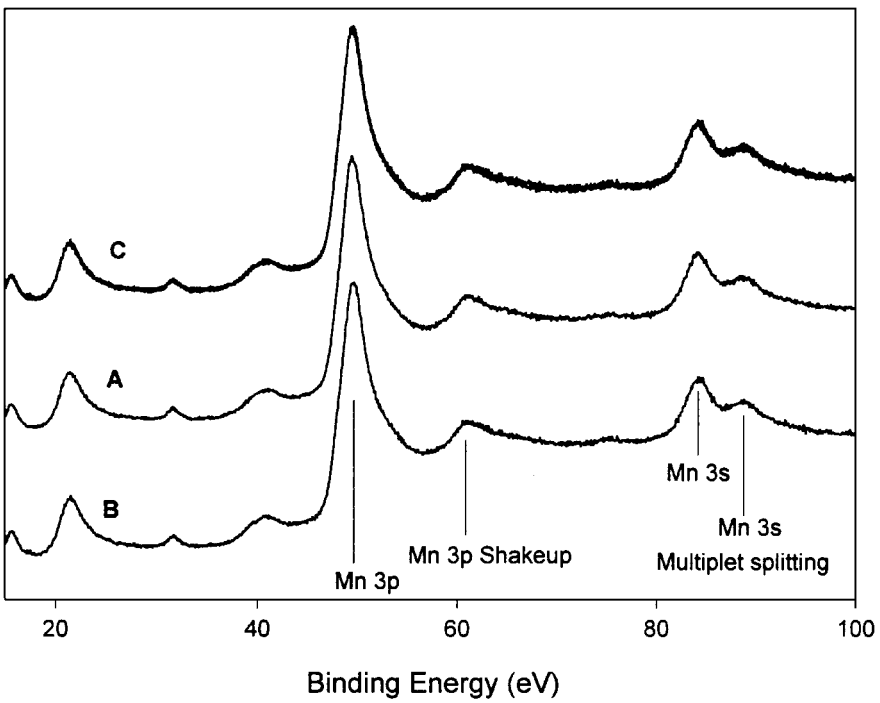

FIG. 11. Comparisons of XPS of Co–A Mn3*s* before and after exposure to H_2/Ar: A, Mn 3*s* spectra before exposure; B, Mn 3*s* spectra after exposure; C, overlay of A and B.

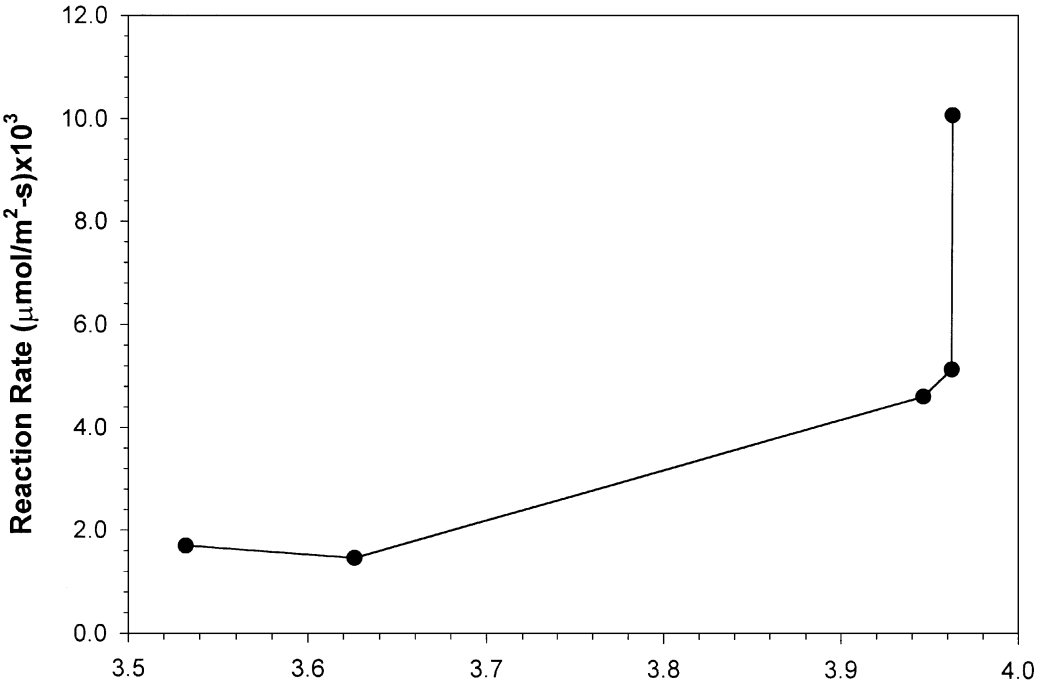

FIG. 12. Dependence of CO oxidation rate upon average oxidation number.

coordinated by six oxygen ions in a rock salt structure. The catalyst of highest activity showed a CO conversion of only 10% at 270°C.

Imamura *et al.* (9) reported that a Mn/Ag (70/30 mole) catalyst shows 80% CO conversion at 100°C and 100% at 150°C at 10,000 vwh. A later publication by Imamura *et al.* (10) showed that addition of 5% Sm to the Mn/Ag catalyst improves the thermal stability of the catalyst, with no change in activity.

Perovskites are mixed oxides with well-documented activity for CO oxidation. For manganite perovskites with Mn^{3+} or Mn^{+4} in octahedral B-sites and La^{3+} (or Sr^{2+}) in dodecahedral A-sites, CO oxidation is significantly lower than for perovskites with Co in B-sites (12, 13). However, even with cobaltites, onset temperatures for CO oxidation (conversion around 1%) are about 75°C. With the most active material, CO conversion is only about 60% at 150°C and 7500 vwh. Manganite perovskites catalysts show very low activity.

Au/MnO_x catalysts show very high activity for CO oxidation above 50°C. The Au/MnO_x catalyst results in an initial CO conversion of about 90% at 75°C and 12,000 h^{-1} and remains active at about 75–80% CO conversion within a period of 40–160 h (15). Au/MnO_x catalysts give a CO conversion of 70–80% at 50°C and 12,000 h^{-1} (42). However, a high loading of noble metal (Au) is needed. Hoflund (43) observed an optimum gold content of 10 at.% on MnO_x. In view of the high atomic weight of Au, such a high gold loading seems less attractive, as compared to a very low loading of Co and Ag on doped OMS-2 catalysts.

The Ag–B OMS catalyst has higher activity for CO oxidation than Mn/Ag and other catalysts at similar conditions. Cu–A, Cu–C, and Co–A compare favorably with metal and noble metal catalysts reported in the literature.

Plots of the temperature dependence of reaction rates for CO oxidation over Ag–A, Co–A, Cu–A, Cu–C, Co–E and Ag–C catalysts are shown in Fig. 6. Data of Fig. 6 show that different metal loaded OMS materials have markedly different activities at different temperature. These data clearly suggest that the type, amount, and location of various transition metals in OMS catalysts influence their catalytic activity. For example, all transition metal loaded OMS-2 (Co–A, Ag–A, Cu–A, and Cu–C) catalysts have much higher reaction rates than OMS-1 materials (Co–E and Ag–C) within the temperature range we used. Additionally, Ag^{+}-exchanged OMS-2 has the highest reaction rate among all the catalysts. Tests for catalytic activities of those M–OMS-1 catalysts could not be conducted at low temperature (below 60°C) due to low activity.

C. Deactivation of Catalysts and Poisoning by Water Vapor

Temporary poisoning of CO oxidation catalysts by water vapor is frequently reported in many studies. Nearly all base metal catalysts show a decline of activity with long runs. For example, Hopcalite in gas mask filters can operate at ambient temperature, but only for a comparatively short period of time. Loss of Hopcalite activity at room temperature is usually due to poisoning by water vapor and activity is reported to be more stable at 80–90°C (11). Clearfield and

co-workers (7) studied Hopcalite catalysts prepared by different methods and compared catalytic properties of commercial samples obtained from Auergesellshaft. Even the best catalysts showed significant decay in activity within 2 h. For Mn/Ag catalysts (9), CO conversion at 142°C decreases from 98 to 81% when 11% H_2O was added to the feed gas.

Some noble metal catalysts have recently been shown to sustain CO oxidation for over 13 days. For example, Schryer *et al*. (44) reported 98–100% continuous conversion of a stoichiometric mixture of CO and O_2 to CO_2 up to 318 h at 60°C. Hoflund and co-workers (45) later suggest that Au/MnO_x catalysts are superior to Pt/SnO_x catalysts with respect to both activity and stability. For different methods of preparation, especially on carriers other than MnO_x, some supported Au catalysts show a significant decrease in activity during long runs. For example, the activity of a Au/ZrO_2 catalyst (20) showed a decrease of CO conversion by a factor of 3 to 4 over a period of 20 h, if the O_2/CO ratio is larger than stoichiometry. Although catalyst activity can be kept stable at a stoichiometric O_2/CO ratio, the activity level is too low as compared to initial activity at an O_2/CO ratio of 40. A 2.3% Au/TiO_2 catalyst also showed about a 50% activity loss in about 10 h (30). Very recently, Hutchings *et al*. (46) reported that a 6 wt% Au/ZnO can give sustained high activity for the oxidation of CO at ambient temperature for a time on stream of about 12 h.

Doped OMS-2 catalysts are stable during long times on stream. Data of Fig. 3 show that the Cu–A catalyst sustains 100% CO conversion for 4 h at 60°C even with a feed stream that is not dried. All the data of Figs. 1–4 suggest that doped OMS-2 catalysts can achieve high areal rates of CO oxidation over long times on stream up to 30 h. Further experiments at much longer times on stream and with feeds containing CO_2 such as those done with Au catalysts are needed.

D. Stability of Doped OMS-2 Catalysts

From XRD patterns of doped OMS-2 catalysts before reaction, the catalysts seem to be different in crystallinity. In Fig. 7, trace A, the Co–A catalyst gives a clear main diffraction peak of the [112] reflection at 2.39 Å and other peaks from [103], [013], [002], and [411] at 3.07, 2.15, 4.85, and 1.83 Å, respectively, showing the typical structure of cryptomelane. Trace B shows the XRD pattern of the Co–A catalyst after 25 h of time on stream at 100°C. Trace B shows that used Co–A catalysts basically retain their crystalline structure and particle size. The signal to noise ratio (S/N) and peak shapes show minor changes, probably due to slight differences in operation of the diffractometer and smoothing of raw data. Trace C, Fig. 7, shows the XRD pattern of the Ag–B catalyst before reaction. Obviously, the Ag–B catalyst before use is of lower crystallinity than Co–A, see trace C. Trace D, which is an XRD pattern of the Ag–B catalyst after a time on stream of 25 h at 100°C, shows essentially no changes in peak position and intensity of the reflection at 2.39 Å. The peaks at 3.07 and 1.83 Å for the used Ag–B catalyst are split and diminished in intensities. The crystallinity of Cu–A is low even before use. The only discernible peak is at 2.39 Å, see trace E in Fig. 7. The Cu–A catalyst after 6 h time on stream shows (trace F) a slightly enhanced intensity at 2.39 Å. Comparison of the XRD patterns of doped OMS-2 catalysts before and after reaction demonstrates that the catalyst structure is quite stable even after prolonged use.

In Fig. 8, traces A and B are the Mn 2*p* spectra of the Co–A catalyst before and after exposure to $CO + O_2$, respectively. The top trace C, which is an overlay of traces A and B, shows an exact match of these two traces. In Fig. 9, traces A and B show the Co 2*p* spectra before and after exposure to $CO + O_2$, with top trace C also showing an exact match of A and B, after doubling the intensity of the latter. Similarly, traces A and B in Fig. 10 show the O 1*s* spectra before and after exposure, respectively. Both of them show a shoulder at the high binding energy side. The main peaks at lower binding energy (529.5 eV) are assigned to lattice O^{2-} ions. The shoulders at 1.6 eV higher binding energy, can be generally assigned to hydroxyl oxygen or chemisorbed oxygen. An exact match of both the main peaks and the shoulders of traces A and B suggests that either chemisorbed oxygen or hydroxyl group are still present even after exposure to $CO + O_2$ gas mixtures for 1 h. Further experiments are needed to confirm such an assignment.

Rojas *et al*. (47) reported that Mn^{2+}, Mn^{3+}, and Mn^{4+} have essentially the same binding energy for manganite perovskite samples. Lombardo *et al*. (48) reported that Co 2*p* spectra in general are very broad. Only Co^0 can be differentiated from Co^{2+} and Co^{3+} via deconvolution of the 2*p* spectra. This method is rather insensitive for evaluating the separate contributions of Co^{2+} and Co^{3+}, due to the close values of binding energies of the two broad peaks. The coincidence of the above-mentioned XPS spectra before and after exposure to $CO + O_2$ or H_2 cannot give information of changes in valence states of Co and Mn. However, Lombardo *et al*. (48) indicated that the appearance of two shake-up satellite peaks of Co 2*p* are characteristic of Co^{2+} and can be considered as fingerprints of this ion, since Co^{3+} shows the absence of shake-up satellites in the Co 2*p* spectra.

For Mn XPS, detailed studies of Shirley (49) have shown that the experimental binding energies for the 3*s* multiplet splitting of the Mn ion depends upon the number of 3*d* electrons. The least oxidized Mn^{2+} ($3d^5$) species show a peak, which is 7 eV higher in binding energy than the main peak of Mn^{2+} ions. The multiplet-splitting peak shifts 1 eV lower in energy as the number of 3*d* electrons is decreased. These two criteria for differentiation of different valence states of Mn (by multiplet splitting of Mn 3*s*) and Co (by shake-up

splitting of Co 2*p*) were used in this study. From Fig. 9, the Co 2*p* spectrum clearly shows satellite peaks at 8.5 eV higher than the Co $2p_{3/2}$ peak (780.0 eV), and the satellite peaks in traces A and B show exact coincidence (trace C). From Fig. 11, the Mn 3*s* spectra for the Co–A catalyst, before (trace A) and after exposure (trace B) to H_2, again show an exact match of the multiplet splitting peaks (traces A and B) at 88.6 eV, which is 4.5 eV higher than the Mn 3*s* main peak (see trace C).

Exact matches of the XPS data for samples before and after treatment for all four binding energy regions, together with their shake-up features and multiplet splittings, demonstrate that the Co–A catalyst experiences no change in valence states of Co and Mn after exposure to $CO + H_2$ or H_2. Such matches also suggest that relative surface concentrations among Co, Mn, or O do not change, as the intensities of each peak show no change after exposure to CO or H_2. This further demonstrates the stability of the Co–A catalyst against reduction by CO or H_2 under mild conditions prevalent in our study. This does not exclude charge transfer via redox reactions of cobalt and manganese, as will be discussed later.

E. Competition of CO Oxidation versus H_2 Oxidation

If the O_2/CO in the feed gas that contains hydrogen is of a stoichiometric ratio, this is a challenge for competition of CO oxidation versus H_2 oxidation, especially when H_2 is present in large excess with respect to both CO and O_2. Most studies (16–18, 50) of oxidation of CO and H_2 report a separate comparison of catalytic oxidation of carbon monoxide and hydrogen. One of the earliest studies related to separate oxidation of CO and H_2 over manganese dioxide showed that the oxidation rates for hydrogen exceed those for carbon monoxide (50). Essentially complete loss of oxidation capacity of MnO_2 was observed after about 3 h time on stream. For supported Au, Haruta *et al*. (17, 18) presented data on H_2 and CO oxidation in separate experiments, and this catalyst is also very active for H_2 oxidation. No data were presented for simultaneous reactions of CO, H_2, and O_2 in the feed stream. In another paper by Haruta *et al*. (16), a Mn/Co/Ag composite catalyst was reported to be highly active for the oxidation of CO and H_2, with separate streams of CO and H_2.

Very few reports have been published on oxidation of mixed gases of $CO + H_2$, and nearly all of these were conducted at high oxygen content. Stetter and Blurton (51) reported oxidation of CO and H_2 in a gas mixture containing 200 ppm of CO and 2% of H_2 in air. Platinized asbestos and Pd/SiO_2 used in their study (47) gave similar conversion for both CO and H_2 over a wide range of temperatures. Vlasenko *et al*. (52) studied the effects of the presence of CO and H_2 in oxidation reactions over Pd/MnO_2 and $Pd/CuCr_2O_4$. Data in this paper clearly show that these catalysts are not selective for CO oxidation when hydrogen is present.

Oh and Sinkevitch (53) showed that alumina-supported Ru or Rh catalysts were the most selective catalysts for CO oxidation in a H_2-rich feed gas. With a feed containing 900 ppm CO and 8500 ppm H_2 in N_2, the most active and selective Ru/Al_2O and Rh/Al_2O_2 catalysts at 180°C require 800 ppm of O_2 in the feed to achieve 100% conversion of CO. This means that a significant level of H_2 oxidation occurs which needs more oxygen than the theoretical stoichiometric ratio of 1 : 0.5. Takada (54) reported results of oxidation of H_2/CO mixed gases over Co_3O_4 and other Co-containing spinels. The feed gas used in their study contained 1% CO, 1% H_2, and 5% O_2 in N_2. They reported data relating changes in conversion of CO and H_2 to reaction temperature (54). Even with the most selective catalyst for CO oxidation (Co_3O_4), the H_2 conversion is considerable. In both studies the longevity of the catalyst was not reported.

The selectivity for CO oxidation versus H_2 oxidation over Co–A, as shown in Fig. 5, is unique, not only in its exclusive selectivity to CO oxidation in the presence of a large excess of H_2, but also in the oxygen present in the feed gas is of such a limited amount that even the slightest consumption by H_2 oxidation will exhaust the oxygen supply that is available for CO oxidation resulting in a significant loss of CO conversion. Note that the Co–A catalyst can be operated at a temperature (100°C) more compatible with the operation of solid–polymer–electrolyte fuel cells than many other systems described above.

F. Correlation of Catalytic Activity with Manganese Valence

Many attempts have been made to probe structure–activity relationships of manganese containing catalysts for CO oxidation. Magnetic susceptibility measurements, XRD structure determination, XPS surface studies, infrared techniques, and UV-vis spectroscopic techniques have all provided insight in catalyst characterization. Some fruitful studies are those of Kanungo (5, 6) that discuss surface excess oxygen and available oxygen content. The determinations of surface active oxygen by the reaction of excess KI at a specified pH (7.1) and determinations of surface hydroxyl groups by reaction with KI in DMF media provide information on surface oxygen species. These two reactions may also probe bulk oxygen species.

Titration methods using KI, Fe^{2+}, and oxalate have been conventionally applied for determination of available oxygen in the bulk phase of manganese oxides and have been critically compared for their accuracy (55). With necessary precautions, all of these yield comparably accurate results. We have used methods involving titration of remaining Fe^{2+} against standard $KMnO_4$ solution for the determination of

total Mn^{2+} after dissolving doped OMS samples in excess Mohr's salt solution.

The determination of the population of manganese of different valence states coexisting in solid manganese oxide samples encounters difficulty for the separation of Mn^{2+} and Mn^{3+}. Although a few methods have been suggested for the determination of Mn^{3+} (56, 57), most of these are difficult procedures to conduct.

The determination of Mn^{3+} content in a sample with coexistence of Mn^{2+}, Mn^{3+}, and Mn^{4+} by leaching with dilute HNO_3 and subsequent titration of Mn^{2+} formed from disproportionation of Mn^{3+} (used here) is rather simple and straightforward. The reliability of the extraction of Mn^{2+} and Mn^{3+} with dilute ammonium sulfate and nitric acid, respectively, seems justified by referring to Table 2. The average oxidation numbers, obtained by calculation from amounts of Mn^{2+}, Mn^{3+}, and Mn^{4+} agree very well with the direct determination as shown in Table 2.

A plot of apparent reaction rates at 60°C (in $mol \cdot m^{-2} \cdot s^{-1}$) for CO oxidation over Ag–C, Co–A, Co–E, Cu–A, and Cu–C catalysts versus average oxidation numbers of Mn is shown in Fig. 12. The correlation between the average oxidation state of Mn and reaction rates implies that higher average oxidation numbers lead to higher CO oxidation rates. Kanungo (5, 6) reported a monotonic increase of catalytic activity of mixed $CuO–MnO_2$ for CO oxidation with surface excess oxygen as determined by the KI (pH 7.1) method. The shape of this correlation curve (Fig. 1, Ref. (5)) resembles our data of Fig. 12. However, the catalytic activities of catalysts are affected by many parameters. For example, besides Mn oxidation state, the type and concentration of these loaded cations also play a dominant role in CO oxidation. In addition, the location of these cations in catalysts also apparently affects the activity of catalysts, as mentioned earlier.

Note that the average oxidation number is also related to the amounts of Mn^{3+} and Mn^{4+} in the samples. Although this number could be higher for samples with higher Mn^{4+} content, the presence of considerable amounts of Mn^{3+} can culminate in a significant lowering of the average oxidation number. The Mn^{3+} contents of Co–E and Ag–C are much higher than doped OMS-2 catalysts, and their average oxidation numbers are thus much lower. Consequently, the reaction rates over these two catalysts are much lower.

G. Role of Tunnel Cations and Mn^{4+} in CO Oxidation

It has been inferred that Mn^{3+} is the active site for CO oxidation on Hopcalite catalysts and that the Zener exchange,

$$Cu^{2+} + Mn^{3+} = Cu^{+} + Mn^{4+}, \qquad [1]$$

is responsible for the catalytic oxidation of CO (5). XPS studies of Hopcalite by Kanungo (5) are in line with the Zener exchange. Vepřek *et al.* (58) used chemical shifts and shake-up information on Cu and multiplet splitting on Mn to confirm the predominance of Cu^{2+} and Mn^{3+} in activated Hopcalite and the predominance of Cu^{+} and Mn^{4+} in deactivated Hopcalite. These data are experimental evidence for the existence of charge transfer between Cu and Mn cations, which should occur even more extensively via *M*–O–Mn bridges during CO oxidation over doped OMS-2 catalysts. However, from correlation between activity and average oxidation number, especially from the Mn population determination, it is clear that the presence of higher amounts of Mn^{3+} in doped OMS-2 catalysts lowers their activity. The higher Mn^{4+} content of catalysts leads to higher activity. Our data suggest that either a small amount of Mn^{3+} or a large amount of Mn^{4+} (or both together) are important for high activity of CO oxidation catalysts. Doped OMS-1 catalysts are of much lower activity than OMS-2 systems. The larger 3×3 tunnel size of OMS-1 or the presence of higher Mn^{3+} content might be responsible for diminished shape selectivity.

The presence of Co^{2+}, Ag^{+}, or Cu^{2+} ions in OMS-2 materials is critical. We suggest that charge transfer along *M*–O–Mn bonds (in which *M* stands for Co^{2+}, Ag^{+}, or Cu^{2+}) may be responsible for CO oxidation. The cations in the cryptomelane 2×2 tunnel structure are in an 8-coordinate environment (59). Such 8-coordinated Co^{2+}, Ag^{+}, or Cu^{2+} ions constitute together with 6-coordinated Mn^{4+} ions special *M*–O–Mn bridges for fast electron transfer. The role played by the Zener exchange between *M* (Cu^{2+}, Co^{2+}, and Ag^{+}) and Mn ions (Eq. [1]) may be realized via these oxygen bridges. For example, tunnel cations (Co^{2+}, Ag^{+}, or Cu^{2+}) on one end of the *M*–O–Mn bridge may abstract electrons from oxygen anions which are formed from dioxygen molecules (possibly chemisorbed near the *M*–O–Mn bridge) due to oxidation of CO. Redox reactions take place with reoxidation of oxygen anions back to dioxygen molecules (available for further oxidation of CO) and reduction of the tunnel cations. The reduced tunnel cations are reoxidized by charge transfer from the Mn^{4+} ions on the other end of the bridge through the oxygen bridge. The reduced Mn ions on the bridge are then reoxidized by gaseous oxygen molecules. This constitutes a complete redox cycle, and the *M*–O–Mn bridge facilitates the electron transfer between *M* and Mn along the bridge.

The electron transfer along the *M*–O–Mn bridge must be very rapid. Of course, the XPS study cannot reveal such a rapid transfer. A multiplet split peak occurs at 4.5 eV higher than the Mn 3*s* peak. From Shirley's estimation (49), the Mn should be in the 4+ valence states. The position of the multiplet splitting peak for Mn 3*s* agrees with the value reported by Brabers *et al.* (60) for tetravalent Mn in manganate spinels. The presence of Co 2*p* shake-up satellite peaks of Co–A indicates the predominance of Co^{2+} valence states in Co–OMS-2. The position of the shake-up satellite peak of Co $2p_{3/2}$ agrees with the report of Marcos *et al.*

(61). This means that the Co and Mn remain in their initial valence states of Co^{2+} and Mn^{4+} throughout the catalytic oxidation of CO. It is clear that the Zener exchange between the Co and Mn ions (Eq. [1]) under experimental conditions favors the initial species.

Several questions concerning the control of the average oxidation number and the Mn^{3+} content of doped OMS catalysts by varying preparation conditions to achieve higher catalytic activity still remain. Such studies are currently in progress in our laboratory.

V. SUMMARY

We have shown here that Co-, Ag-, and Cu-doped octahedral molecular sieves with the cryptomelane structure are high activity catalysts for low-temperature CO oxidation. These OMS-2 catalysts exhibited very stable performance over long times on stream, as compared to known Hopcalite-like Cu–Mn mixed oxides and other base metal supported catalysts. Some of the doped OMS-2 catalysts seem to exhibit high resistance to water poisoning and excellent selectivity to CO oxidation versus competition with a large excess of H_2. The stability of doped OMS-2 catalysts was further substantiated by XRD and XPS studies. The activity of these OMS-2 catalysts seems to be dominated both by their average oxidation numbers and by the species and position of the doped cation. A special *M*–O–Mn bridge with suitable coordination in the OMS-2 structure is suggested to be responsible for high activity doped OMS-2 catalysts. A mechanism of CO oxidation on OMS-2 involving reversible electron transfer was proposed.

ACKNOWLEDGMENTS

We acknowledge the Department of Energy, Office of Basic Energy Sciences, Division of Chemical Sciences for support of this research. We thank A. Clearfield, M. Kelly, R. S. Weber, and M. A. Vannice for helpful discussions.

REFERENCES

1. Lamb, A. B., Bray, W. C., and Frazer, J. C. W., *J. Ind. Eng. Chem.* **12**, 213 (1920).
2. Merrill, D. R., and Scalione, C. C., *J. Am. Chem. Soc.* **43**, 1982 (1921).
3. Rogers, T. H. R., Piggot, C. S., Bahlke, W. H. R., and Jennings, J. M., *J. Am. Chem. Soc.* **43**, 1973 (1921).
4. Schwab, G. M., and Kanungo, S. B., *Z. Physik. Chem. (N.F.)* **107**, 109 (1977).
5. Kanungo, S. B., *J. Catal.* **58**, 419 (1979).
6. Kanungo, S. B., *Indian J. Chem. A* **26**, 373 (1987).
7. Puckhaber, L. S., Cheung, H. R., Cocke, D. L., and Clearfield, A., *Solid State Ionics* **32/33**, 206 (1989).
8. Wright, P. A., Natarajan, S., Thomas, J. M., and Gai-Boyes, P. L., *Chem. Mater.* **4**, 1053 (1992).
9. Imamura, S., Sawada, H. R., Uemura, K., and Ishida, S., *J. Catal.* **109**, 198 (1988).
10. Imamura, S., Yoshie, S., and Ono, Y., *J. Catal.* **115**, 258 (1989).
11. Solov'ev, S. A., Belokleitseva, G. M., and Vlasenko, V. M., *Zh. Prikl. Khim.* **65**(9), 1921 (1992).
12. Voorhoeve, R. J. H. R., Johnson, D. W., Jr., Remeika, J. P., and Gallagher, P. K., *Science* **195**, 827 (1977).
13. Chan, K. S., Ma, J., Jaenicke, S., and Chuah, G. K., *Appl. Catal. A* **107**, 210 (1994).
14. Gardner, S. D., Hoflund, G. B., Upchurch, B. T., Schryer, D. R., Kielin, E. J., and Schryer, J., *J. Catal.* **129**, 114 (1991).
15. Gardner, S. D., Hoflund, G. B., Schryer, D. R., Schryer, J., Upchurch, B. T., and Kielin, E. J., *Langmuir* **7**, 2135 (1991).
16. Haruta, M., and Sano, H. R., *Stud. Surf. Sci. Catal.* **16**, 225 (1983).
17. Haruta, M., Yamada, N., Kobayashi, T., and Iijima, S., *J. Catal.* **115**, 301 (1989).
18. Haruta, M., Tsubota, S., Kobayashi, T., Kageyama, H. R., Genet, M., and Delmon, B., *J. Catal.* **144**, 175 (1993).
19. Haruta, M., Tsubota, S., Kobayashi, T., Ueda, A., Sakurai, H. R., and Ando, M., *in* "Proc. 10th International Congress on Catalysis, Budapest, 1992" (L. Guczi, F. Solymosi, and P. Tetenyi, Eds.), p. 2657. Akadémiaikiadó, Budapest, 1993.
20. Knell, A., Barnickel, P., Baiker, A., and Wokaun, A., *J. Catal.* **137**, 306 (1992).
21. Schryer, D. R., Upchurch, B. T., van Norman, J. D., Brown, K. G., and Schryer, J., *J. Catal.* **122**, 193 (1990).
22. Gardner, S. D., Hoflund, G. B., Davidson, M. R., Laitnen, H. R. A., Schryer, D. R., and Upchurch, B. T., *Langmuir* **7**, 2140 (1991).
23. Schryer, D. R., Upchurch, B. T., Sidney, B. D., Brown, K. G., Hoflund, G. B., and Herz, R. K., *J. Catal.* **130**, 314 (1991).
24. Choi, K. I., and Vannice, M. A., *J. Catal.* **127**, 465 (1991).
25. Choi, K. I., and Vannice, M. A., *J. Catal.* **127**, 489 (1991).
26. Choi, K. I., and Vannice, M. A., *J. Catal.* **131**, 1 (1991).
27. Choi, K. I., and Vannice, M. A., *J. Catal.* **131**, 22 (1991).
28. Choi, K. I., and Vannice, M. A., *J. Catal.* **131**, 36 (1991).
29. Bollinger, M. A., Thesis, Pennsylvania State Univ., 1994.
30. Lin, S. D., Bollinger, M., and Vannice, M. A., *Catal. Lett.* **17**(3–4), 245 (1993).
31. Grunwaldt, J.-D., Kiener, C., Wogerbauer, C., and Baiker, A., *J. Catal.* **181**, 23 (1999).
32. Grunwaldt, J.-D., and Baiker, A., *J. Phys. Chem. B* **103**, 1002 (1999).
33. *Chem. Eng. News* Jan. 13, 20 (1997).
34. Taguchi, H. R., Ohota, A., and Nagao, M., *J. Mater. Sci.* **31**, 5697 (1996).
35. Shen, Y. F., Suib, S. L., and O'Young, C. L., *J. Catal.* **161**, 115 (1996).
36. Dietz, W. A., *J. Gas Chrom.* **5**, 68 (1967).
37. Shen, Y. F., Suib, S. L., and O'Young, C. L., *J. Am. Chem. Soc.* **116**(24), 11020 (1994).
38. DeGuzman, R. N., Awaluddin, A., Shen, Y. F., Tian, Z. R., Suib, S. L., Ching, S., and O'Young, C. L., *Chem. Mater.* **7**(7), 1286 (1995).
39. Suib, S. L., *Stud. Surf. Sci. Catal.* **102**, 47 (1996).
40. Parida, K. M., Kanungo, S. B., and Sant, B. R., *Thermochim. Acta* **26**, 435 (1981).
41. Glover, D., Schumm, B., Jr., and Kozawa, A., Eds., "Handbook of Manganese Dioxide Battery Grade." International Battery Material Association, 1989.
42. Hoflund, G. B., and Gardner, S. D., *Langmuir* **11**, 3431 (1995).
43. Hoflund, G. B., Gardner, S. D., Schryer, D. R., Upchurch, B. T., and Kielin, E. J., *Appl. Catal. B* **6**(2), 117 (1995).
44. Schryer, D. R., Sidney, B. D., Miller, I. M., Hess, R. V., Wood, G. M., Batten, C. E., Burney, L. G., Hoyt, R. F., and Paulin, P. A., NASA Conf. Publ., No. 2458, 113, 1987.
45. Hoflund, G. B., Gardner, S. D., Schryer, D. R., Upchurch, B. T., and Kielin, E., *J. React. Kinet. Catal. Lett.* **58**(11), 19 (1996).
46. Hutchings, G. J., Siddiqui, M. R. H. R., Burrows, A., Kiely, C. J., and Whyman, R., *J. Chem. Soc. Faraday Trans.* **93**, 187 (1997).

47. Rojas, M. L., Fierro, J. L. G., Tejuca, L. G., and Bell, A. T., *J. Catal.* **124**, 41 (1990).
48. Lombardo, E. A., Tanaka, K., and Toyoshima, I., *J. Catal.* **80**, 340 (1983).
49. Shirley, D. A., *Phys. Scrip.* **11**(3/4), 117 (1975).
50. Brooks, C. S., *J. Catal.* **8**, 272 (1967).
51. Stetter, J. R., and Blurton, K. F., *Ind. Eng. Chem. Prod. Res. Dev.* **19**, 214 (1980).
52. Vlasenko, V. M., Lunev, N. K., and Kurilets, Ya. P., *Ukr. Khim. Zh.* **48**(4), 366 (1982).
53. Oh, S. H. R., and Sinkevitch, R. M., *J. Catal.* **142**, 254 (1993).
54. Takada, T., Kasahara, S., Omata, K., and Yamada, M., *Nippon Kagaku Kaishi* **9**, 793 (1994).
55. Murray, J. W., Balistrieri, L. S., and Paul, B., *Geochim. Cosmochim. Acta* **48**, 1237 (1984).
56. Fyfe, W. S., *Anal. Chem.* **23**, 174 (1951).
57. Laitinen, H. R., Zhou, H. R., and Mitamura, S., *Prog. Batteries Solar Cells* **9**, 136 (1951).
58. Veprek, S., Cocke, D. L., Kehl, S., and Oswald, H. R. R., *J. Catal.* **100**, 250 (1986).
59. Post, J. E., von Derrle, R. B., and Buseck, P. R., *Acta Cryst. B* **38**, 1056 (1982).
60. Brabers, V. A. M., van Setten, F. M., and Knapen, P. S. A., *J. Solid State Chem.* **49**, 93 (1983).
61. Marcos, J. A., Buitrago, R. H. R., and Lombardo, E. A., *J. Catal.* **105**, 95 (1987).